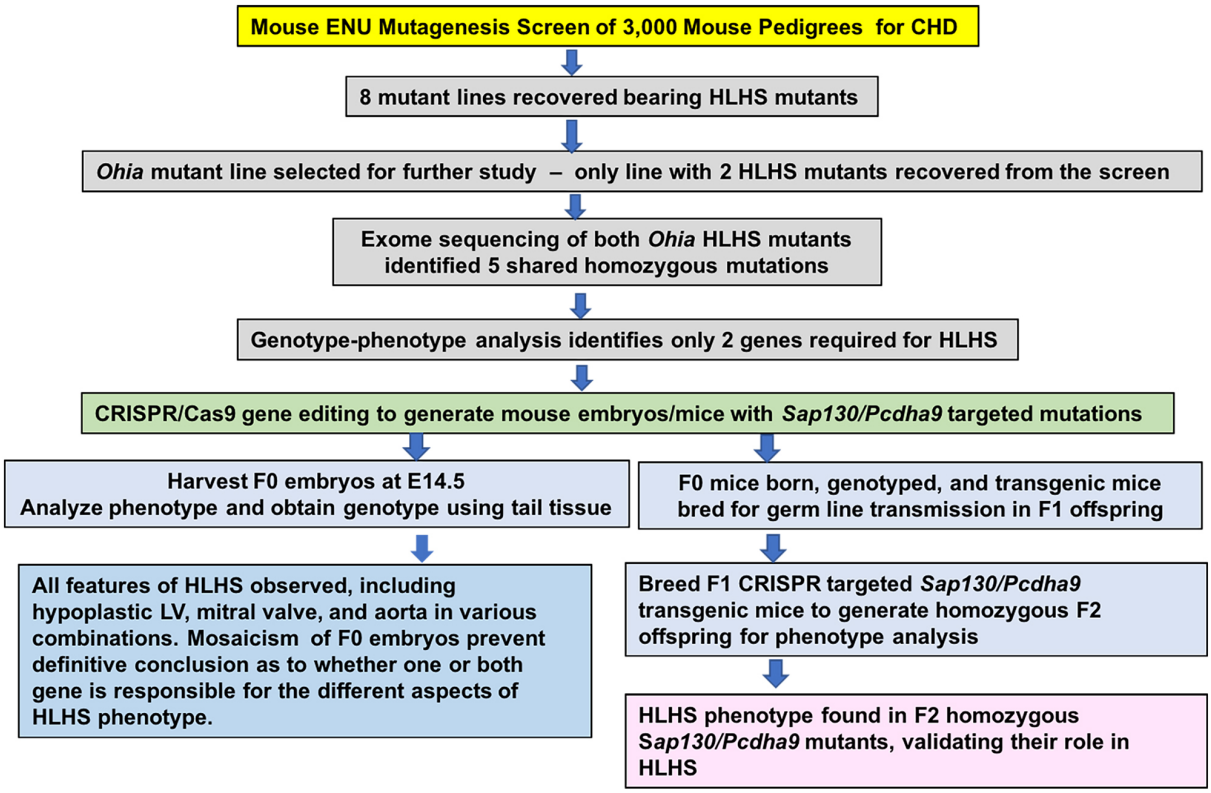

Supplementary Figure 1. Recovery of *Sap130* and *Pcdha9* mutations as causative for HLHS in *Ohia* mutant line

Flow chart showing recovery of HLHS mutants from the mouse forward genetic screen and the analysis undertaken that identified mutations in *Sap130* and *Pcdha9* as causative for HLHS.

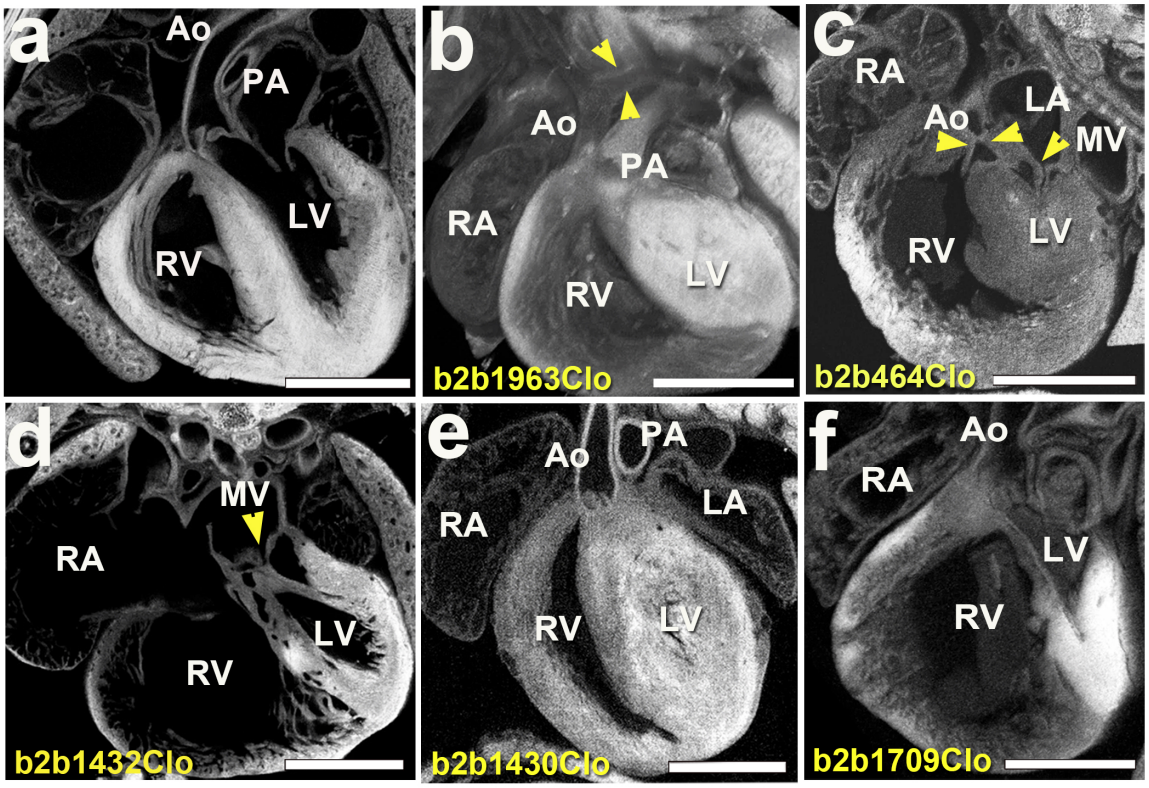

Supplementary Figure 2. **HLHS phenotype in five independent mutant mouse lines recovered from the mutagenesis screen**

Histopathology showing a normal mouse heart (a) and the hearts of 5 independently derived HLHS mutants (b-f) with the JAX Mouse Genome Informatics mutant line ID indicated (http://www.informatics.jax.org/). Note the small size of the LV with little or no lumen in the HLHS mutants. In the HLHS mutants shown in (b), (c), and (e), the LV is muscle bound. Arrowheads in (b) denote hypoplastic aortic arch, in (c) hypoplastic aorta and stenotic mitral valve, and in (d) hypoplastic mitral valve.

Ao, Aorta; PA, pulmonary artery; LV, left ventricle; RV, right ventricle; MV, mitral valve; LA, left atrium; RA, right atrium; Scale bar=1mm.

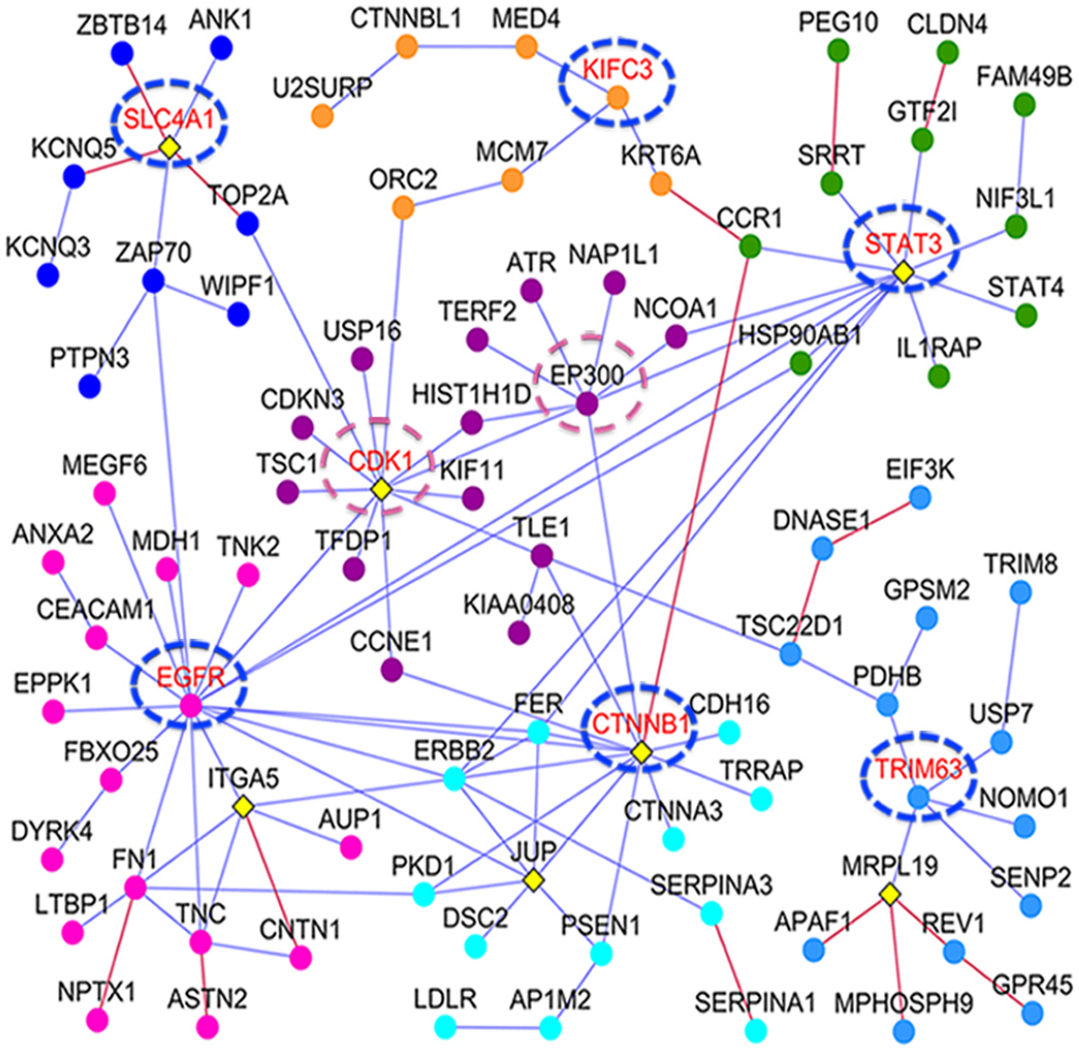

Supplementary Figure 3. Network analysis of mouse HLHS mutations

Network analysis of mutations recovered from 8 HLHS mouse lines identified 7 interconnected modules comprising 88 of the mouse HLHS genes and 7 linker genes. Each Netbox module is defined by the gene with highest connectivity and is coded by a different color, with linker genes illustrated as yellow diamonds. Note one module (dark purple) has two genes delineated, primary being *CDK1* with the highest connectivity, and *EP300* being secondary with the second highest connectivity. These identified as significantly affected pathways, cell cycle (KIFC3, CDK1), chromatin (EP300), muscle differentiation (TRIM63), mPTP closure, mitochondrial metabolism

and Notch signaling (STAT3,EGFR,EP300), cell adhesion signaling (CTNNB1), growth factor signaling (EGFR,CTNNB1), and cardiac hypertrophy (SLC4A1,TRIM63,EGFR).

Nature Genetics: doi:10.1038/ng.3870

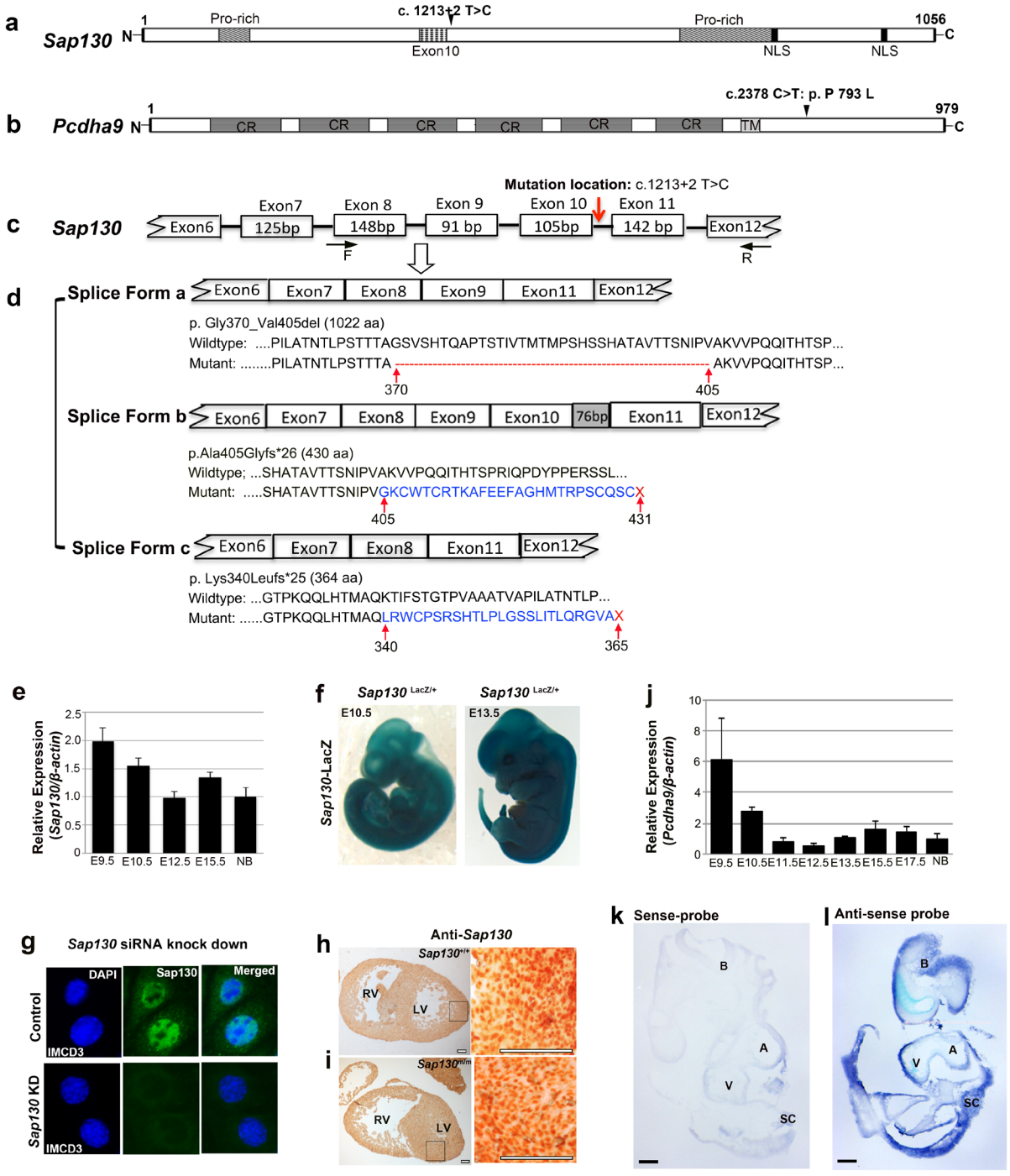

Supplementary Figure 4. *Ohia Sap130/Pcdha9* mutations and developmental profile of *Sap130* and *Pcdha9* expression

(a,b). *Sap130* and *Pcdha9* mutations recovered in the *Ohia* HLHS mutant line (black arrows). Pro-rich:proline-rich, NLS:nuclear localization signal, CR:cadherin repeats, TM:transmembrane.

(c,d). *Sap130* splicing mutation indicated with red arrowhead. Forward (F) and reverse (R) primers used for cDNA amplification indicated by black arrows(c). Three alternatively spliced *Sap130* transcripts from the *Ohia* mutant are shown (d). The predominant alternatively spliced *Sap130* transcript (Splice Form a) causes exon 10 deletion, resulting in 36 amino acid in-frame deletion. Splice form b has a 76 bp insertion in intron10 and splice form c has exons 9 and 10 deletions, both resulting in frameshift with premature termination.

(e). Quantitative PCR analysis of wildtype heart show peak *Sap130* transcript expression at E9.5. Shown are mean±s.d (n=3 technical replicates).

(f). *Sap130* expression was examined using a *Sap130-lacZ* knockout (KO)-first allele (www.komp.org). X-gal staining showed ubiquitous LacZ expression from the *Sap130-LacZ* knockin allele in E10.5 and E13.5 embryos, indicating *Sap130* is broadly expressed in development.

(g). Sap130 antibody staining showed nuclear localization of Sap130 in IMCD3 cells. *Sap130* small interfering RNA knock down (KD) resulted in loss of Sap130 immunostaining, confirming specificity of the Sap130 antibody.

(h,i). Immunohistochemistry showed Sap130 is ubiquitously expressed and is nuclear localized in both wildtype (h) and *Ohia* mutant (i) hearts. Box regions in (h) and (i) are enlarged on the right.

(j). Quantitative PCR analysis of the wildtype heart showed *Pcdha9* transcript expression in the heart is highest at E9.5. Data shown are mean±s.d (n=3 technical replicates).

(k, l). In situ hybridization of E9.5 mouse embryo cryosections with *Pcdha9* antisense and sense probes indicated *Pcdha9* expression in the brain (B), spinal cord (SC), and heart ventricle (V) and atrium (A). Scale bar=100um.

Nature Genetics: doi:10.1038/ng.3870

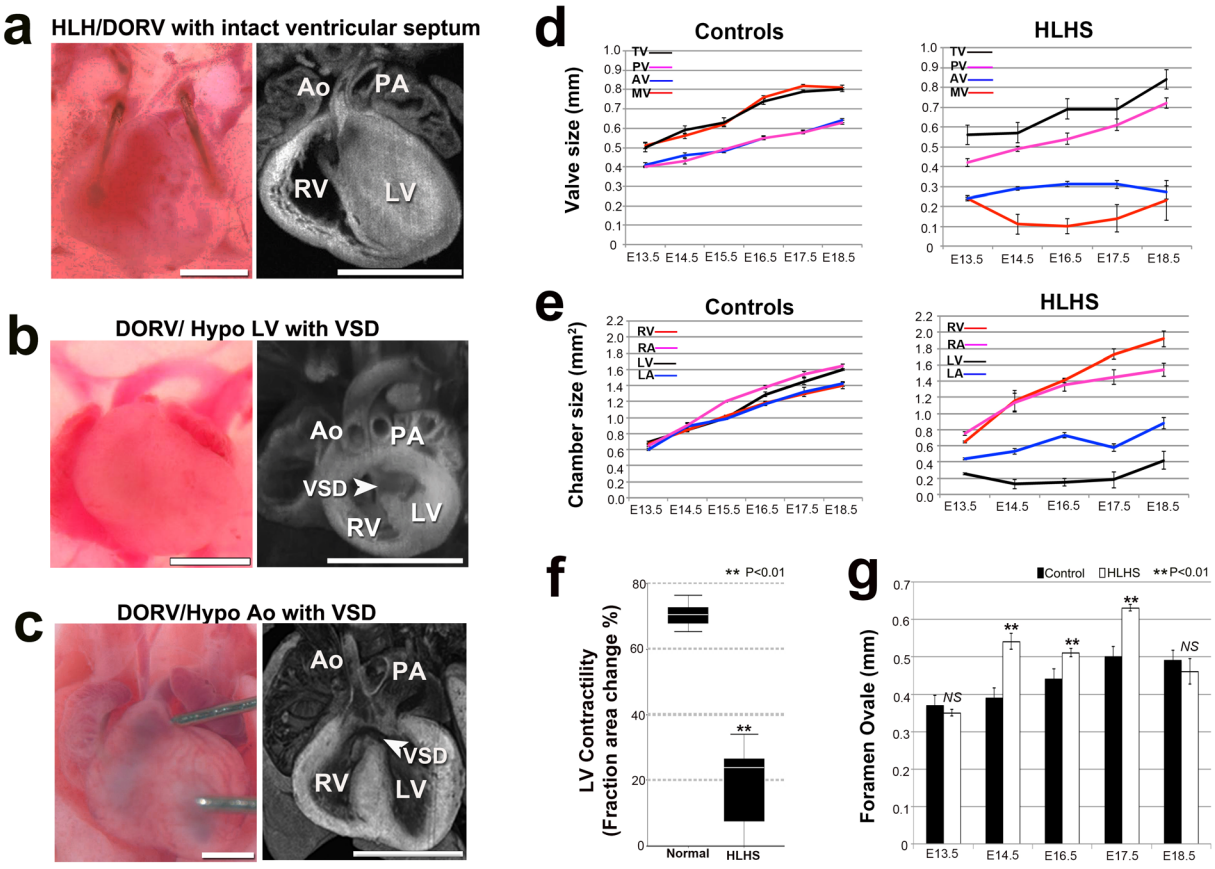

Supplementary Figure 5. HLHS and other CHD phenotypes in the *Ohia* mutant line

(a-c) *Ohia* mutants with isolated hypoplasia of the aorta or LV.

Some *Ohia* mutants exhibit DORV with hypoplasia of both the aorta and LV (a), while others can exhibit DORV with hypoplastic LV, but normal sized Ao (b), or DORV with hypoplastic aorta, but normal LV (c). These independent occurrences of hypoplasia of the LV vs. Ao would suggest these anatomical defects are not hemodynamically driven in *Ohia* mutants. Scale bar, 1 mm.

(d-g). Delineating cardiac development in *Ohia* HLHS mutants using fetal echocardiography

(d,e). Developmental profile of the growth of cardiac valves and chambers in normal vs HLHS embryos (n=15 embryos per group). Data shown are mean±s.e.m.

LA, left atrium; LV, left ventricle; RA, right atrium, RV, right ventricle; MV, mitral valve, TV, tricuspid valve, AV, aortic valve, PV, pulmonary valve.

Nature Genetics: doi:10.1038/ng.3870

(f) Fetal ultrasound measurements show LV contractility is decreased in HLHS mutant fetuses (n=15 embryos per group). Data shown are median with interquartile range. Wilcoxon rank sum test, P=0.000003.

(g) Measurements of the foramen ovale (FO) showed FO size was not restrictive in HLHS mutants. Data shown are mean±s.e.m. Unpaired Student's t-test: E13.5, n=12 (control=6, HLHS=6) P=0.385, t=-0.908, df=10; E14.5, n=18 (control=12, HLHS=6), P=0.000084, t=5.222, df=16; E16.5, n=27 (control=15, HLHS=12), p=0.001, t=3.7, df=25; E17.5, n=21 (control=12, HLHS=9), P=3.4633E-9, t=10.262, df=19; E18.5, n=12 (control=6, HLHS=6), P=0.453, t=-0.782, df=10. NS, not significant.

Nature Genetics: doi:10.1038/ng.3870

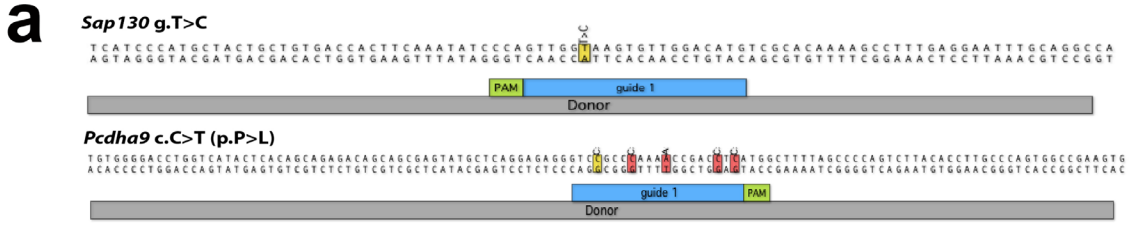

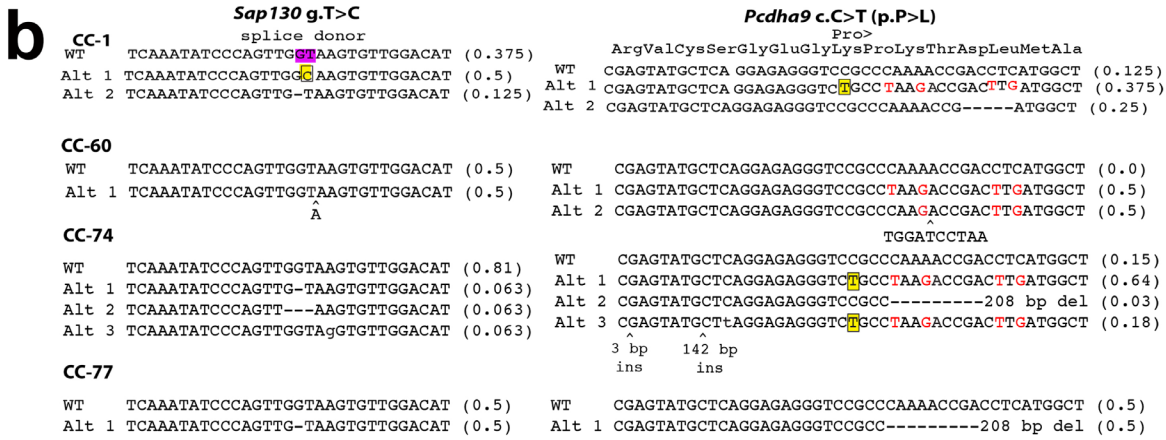

c **F0 *Sap130/Pcdha9* CRISPR/Cas9 Targeted Transgenic Embryos**

Genotype N=52	Ao hypoplasia	LV/MV hypoplasia	Ao/LV/MV hypoplasia	Total with CHD
Sap130 NHEJ (n=3)	0	1	0	1 (33%)
Sap130 KI (n=1)	0	1	0	1 (100%)
Pcdha9 NHEJ (n=23)	2	6	0	8 (35%)
Pcdha9 KI/NHEJ (n=2)	0	0	0	0
Pcdha9 KI (n=10)	0	0	0	0 (0)
Sap130 NHEJ: *Pcdha9* NHEJ (n=5)	1	2	0	3 (60%)
Sap130 NHEJ: *Pcdha9* KI (n=1)	0	1	0	1 (100%)
Sap130 KI/NHEJ: *Pcdha9* KI/NHEJ (n=1)	0	1	0	1 (100%)
Sap130 KI: *Pcdha9* KI (n=1)	0	1	0	1 (100%)
Sap130 KI/NHEJ: *Pcdha9* NHEJ (n=1)	0	1	0	1 (100%)
Sap130 NHEJ: *Pcdha9* KI/NHEJ (n=4)	0	1	1	2 (50%)
TOTAL	3 (6%)	15 (29%)	1 (2%)	19 (37%)

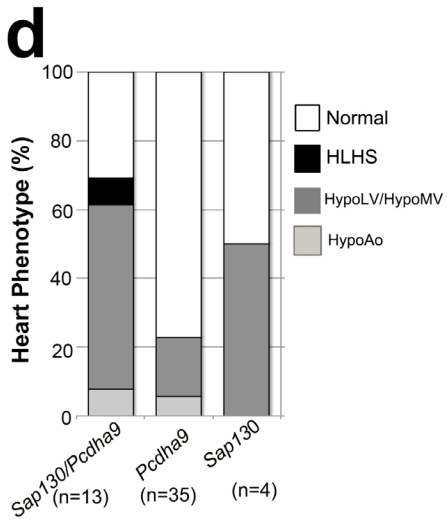

Supplementary Figure 6. Mouse CRISPR/Cas9 targeting of *Sap130* and *Pcdha9* mutations

(a). RNA guides used for CRISPR/Cas9 knockin of *Ohia Sap130* and *Pcdha9* point mutations.

(b). Sequencing analysis of individual F0 embryos generated from zygote injections to achieve CRISPR/Cas9 targeting of the *Sap130* and *Pcdha9* mutations.

(c). Genotype-phenotype summary of transgenic embryos generated by CRISPR/Cas9

Sap130/Pcdha9 targeting. Of the 90 embryos generated, 52 (58%) had at least one gene targeting event, 19 of which had one or more of the three features of HLHS. Also observed was isolated DORV in 1 *Sap130*, 3 *Pcdha9*, and 1 *Sap130/Pcdha9* CRISPR/Cas9 targeted embryo.
(d). Distribution of cardiac phenotypes in *Sap130*/*Pcdha9* CRISPR/Cas9 targeted F0 embryos examined at E14.5.
NHEJ: nonhomologous end-joining; KI: knockin; HypoLV, hypoplastic left ventricle; HypoMV, hypoplastic mitral valve; HypoAo, hypoplastic aorta.

Nature Genetics: doi:10.1038/ng.3870

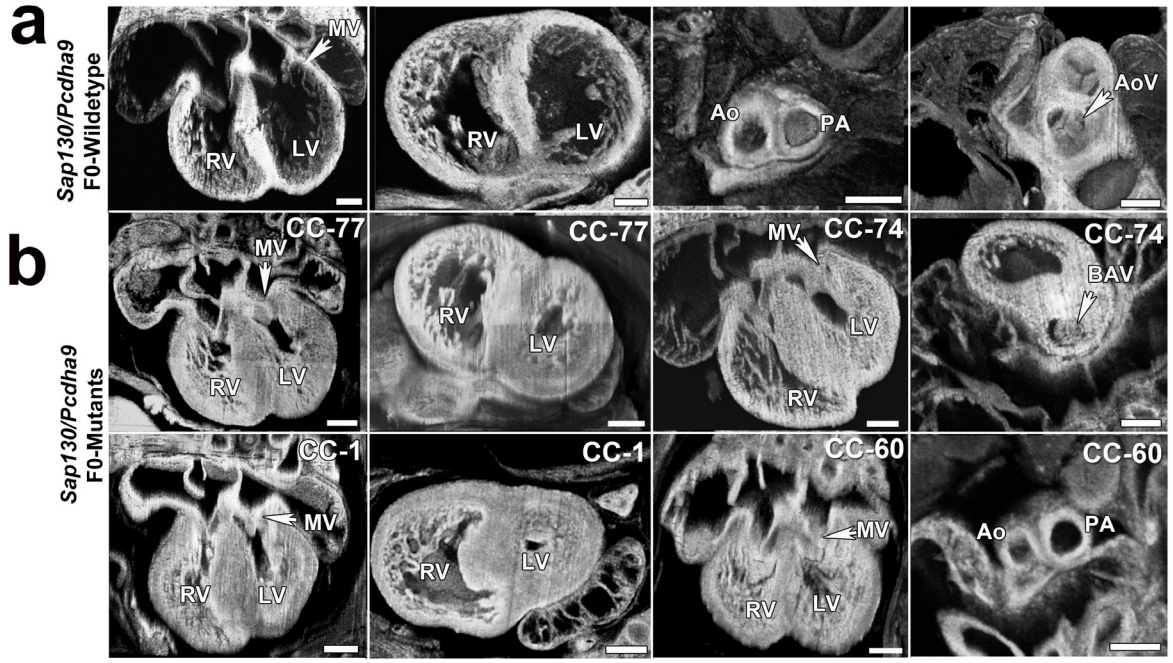

Supplementary Figure 7. Cardiac defects in F0 mouse embryos with CRISPR/Cas9 targeting of *Sap130* and *Pcdha9*

F0 mouse embryos homozygous for CRISPR/Cas9 *Sap130*/*Pcdha9* targeted alleles were harvested and analyzed at E14.5. Four such embryos are shown in (b) with a spectrum of cardiac phenotypes reminiscent of HLHS, including hypoplastic LV, cushion-like thickened mitral valve and narrow aorta. In embryo CC-74, the full spectrum of defects associated with HLHS was observed, including hypoplastic LV, bicuspid aortic stenosis and hypoplastic aorta (b). The normal heart structure of wildtype littermate embryo is shown for comparison in (a). Scale bar, 0.2mm.

Nature Genetics: doi:10.1038/ng.3870

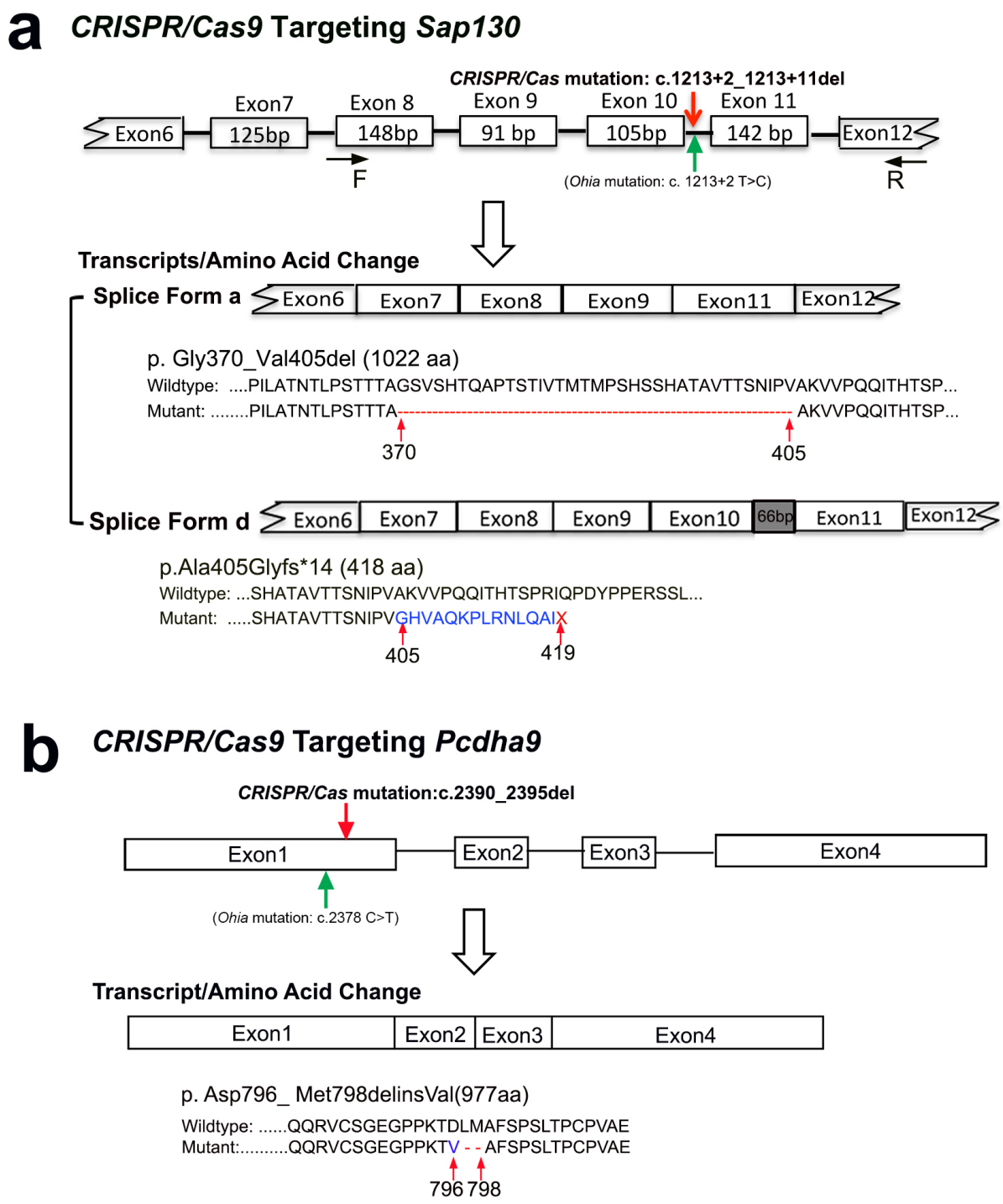

Supplementary Figure 8. **CRISPR/Cas9 targeted mouse *Sap130* and *Pcdha9* Alleles**

A transgenic mouse line was generated with CRISPR/Cas9 gene edited *Sap130* and *Pcdha9* alleles. The *Sap130* and *Pcdha9* alleles are shown above and described in more detail below. Breeding mice carrying these CRISPR targeted *Sap130/Pcdha9* allele generated double homozygous mutants exhibiting HLHS.

(a). CRISPR/Cas9 targeted *Sap130* allele.

The CRISPR gene edited *Sap130* allele is situated at the same position as the *Ohia Sap130* mutation (green arrow), except it encompasses an 11-base deletion. This resulted in two alternatively spliced transcripts. One is identical to the exon 10-in frame deletion seen in *Ohia* encoding a protein with a 36-amino acid in frame deletion (splice form a). Another alternative transcript observed comprised a 66 bp insertion in intron10 that causes premature termination.

(b). CRISPR/Cas9 targeted *Pcdha9* allele.

The *Pcdha9* point mutation in the *Ohia* mutant line is indicated with green arrow, while the CRISPR/Cas9 generated *Pcdha9* mutation is indicated in red. The CRISPR generated mutation resulted in a single amino acid insertion in conjunction with a two amino acids deletion.

Nature Genetics: doi:10.1038/ng.3870

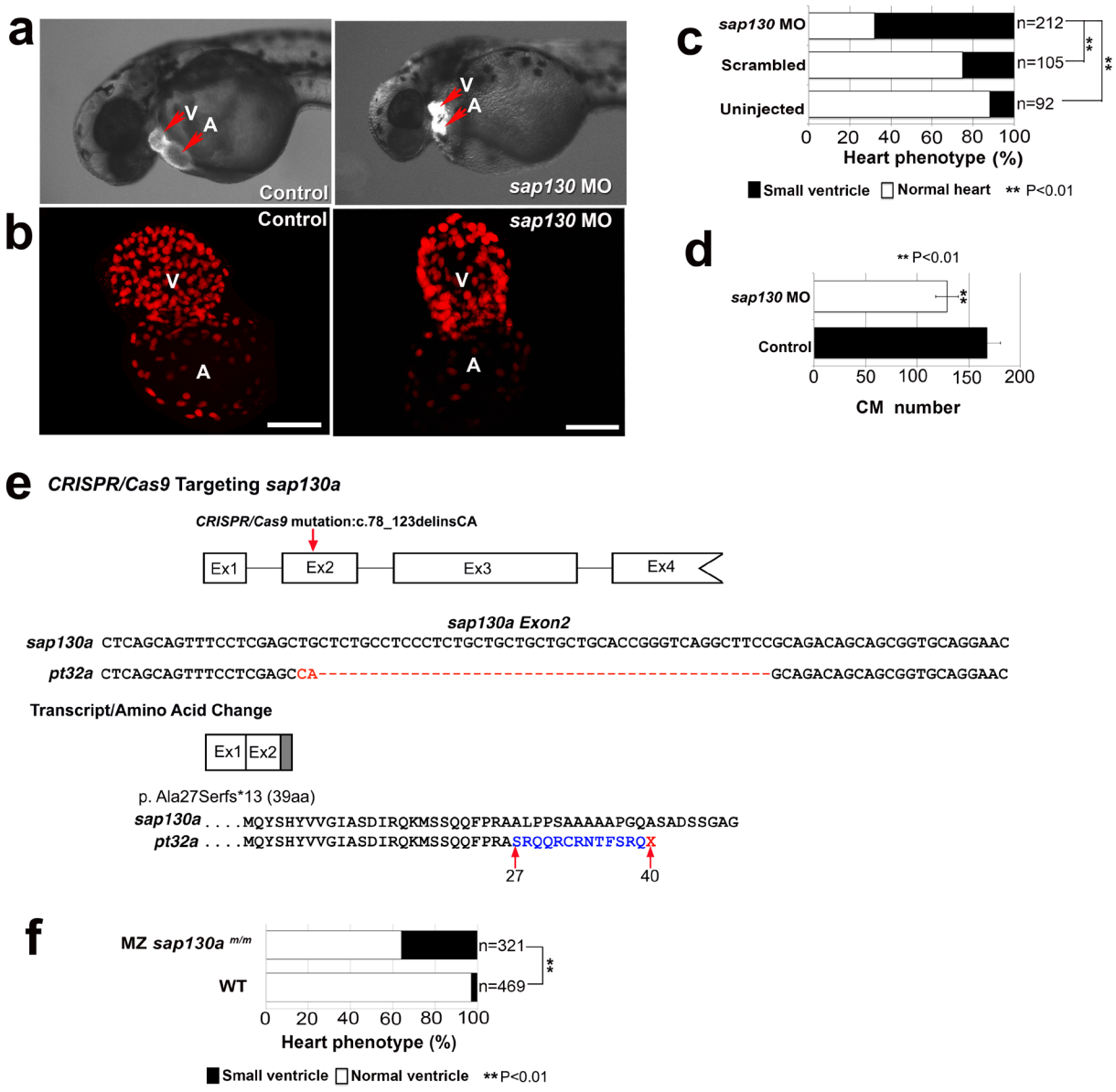

Supplementary Figure 9. Small ventricle in *Sap130*a morpholino knockdown and CRISPR/Cas9 targeted *sap130a* mutant embryos

(a). *sap130a* morpholino (MO) knockdown in zebrafish embryos showed reduction in ventricle size (right panel) when compared to uninjected or scrambled MO injected embryos.

(b). The smaller ventricle phenotype is readily visualized using DsRed cardiomyocyte nuclear labeling (*Tg(5.7myl7:nDsRed2)* in the ventricle at 72hpf (bottom).

(c). *sap130a* MO knockdown of zebrafish embryos at 5 ng MO (n=212) resulted in small heart phenotype compared to scrambled (n=105, Fisher's exact test, P=2.7601E-13) and uninjected

zebrafish embryos (c) (n=92, Fisher's exact test, P=1.7789E-20).

(d). Quantification of DsRed2-labeled cardiomyocyte nuclei showed the *sap130a* MO knockdown (5 ng MO) zebrafish embryos (n=7) had fewer cardiomyocytes compared to control uninjected (n=6). Data shown are mean±s.e.m. Unpaired Student's T-test, P=0.000132, t=5.731, df=11.

(e). CRISPR/Cas9 generated *sap130a* mutation with 2bp insertion and 46bp deletion in exon 2 in zebrafish mutant line pt32a is shown (red arrow), predicting a frameshift causing premature termination.

(f). Homozygous maternal zygotic CRISPR/Cas9 *sap130a* mutant embryos showed small ventricle phenotype (n=321) compared to wildtype zebrafish embryos (n=469; Fisher's exact test, P=8.2846E-37). It was necessary to F4 generate *sap130a* maternal zygotic mutant embryos, as *sap130a* is expressed as maternal transcripts.

V, ventricle; A, atrium. Scale bar, 40μm.

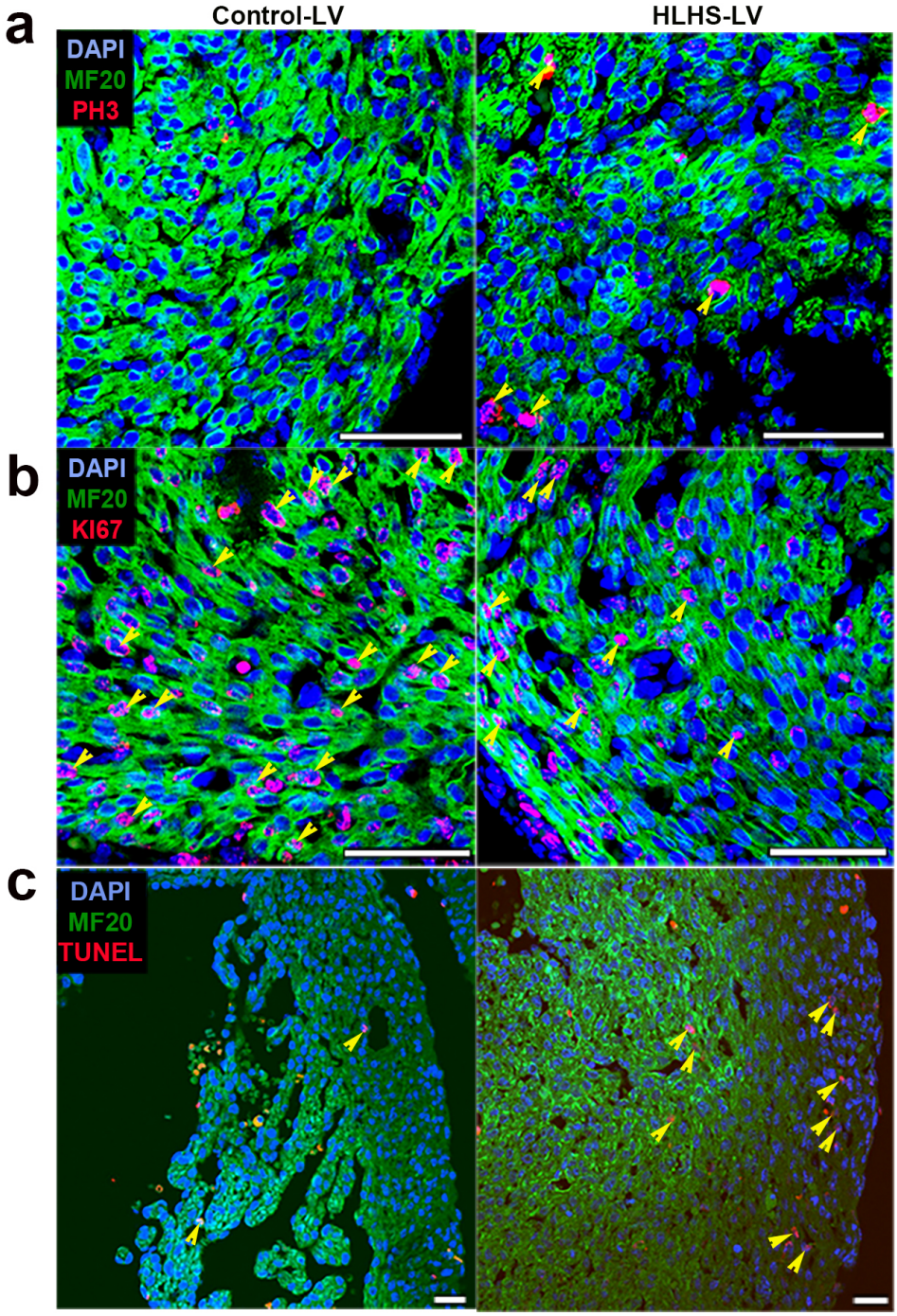

Supplementary Figure 10. Analysis of myocardial cell proliferation and apoptosis in *Ohia* HLHS mutant heart

Immunostaining *Ohia* HLHS mutant and littermate control heart tissue sections were carried out to examine cardiomyocyte cell proliferation and cell death. This entailed conducting immunostaining

with (a) MF20 and phospho-histone H3 (PH3), (b) MF20 and Ki67, and MF20 and TUNEL(c). Arrowheads indicate double positive cells. Scale bar=50um.

Nature Genetics: doi:10.1038/ng.3870

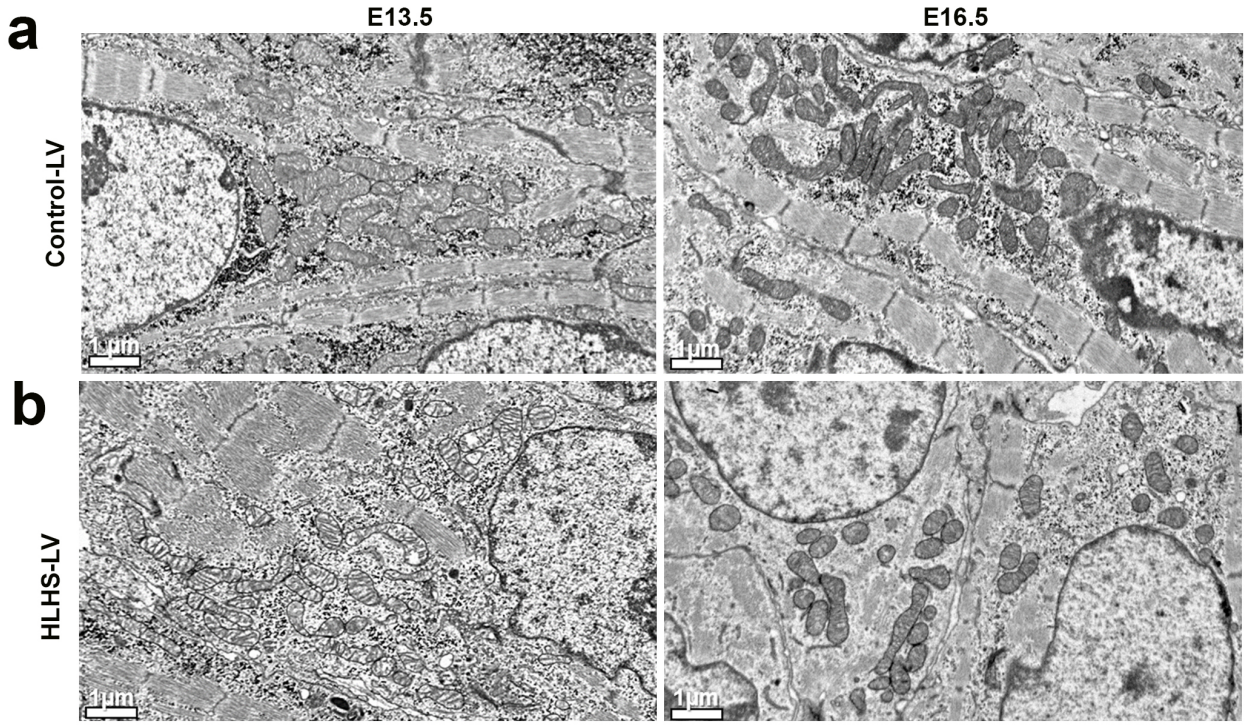

Supplementary Figure 11. Electron microscopy of *Ohia* HLHS-LV

(a,b). Electron microscopy of E13.5 and E16.5 HLHS-LV (b) vs. control-LV (a). HLHS-LV at E13.5 and E16.5 exhibited shorter myofibrils with less distinct z-bands. Mitochondria in HLHS-LV were smaller and elongated at E13.5, but becoming more rounded at E16.5 and have mitochondria with low density matrix and sparse cristae. Scale bar: 1um.

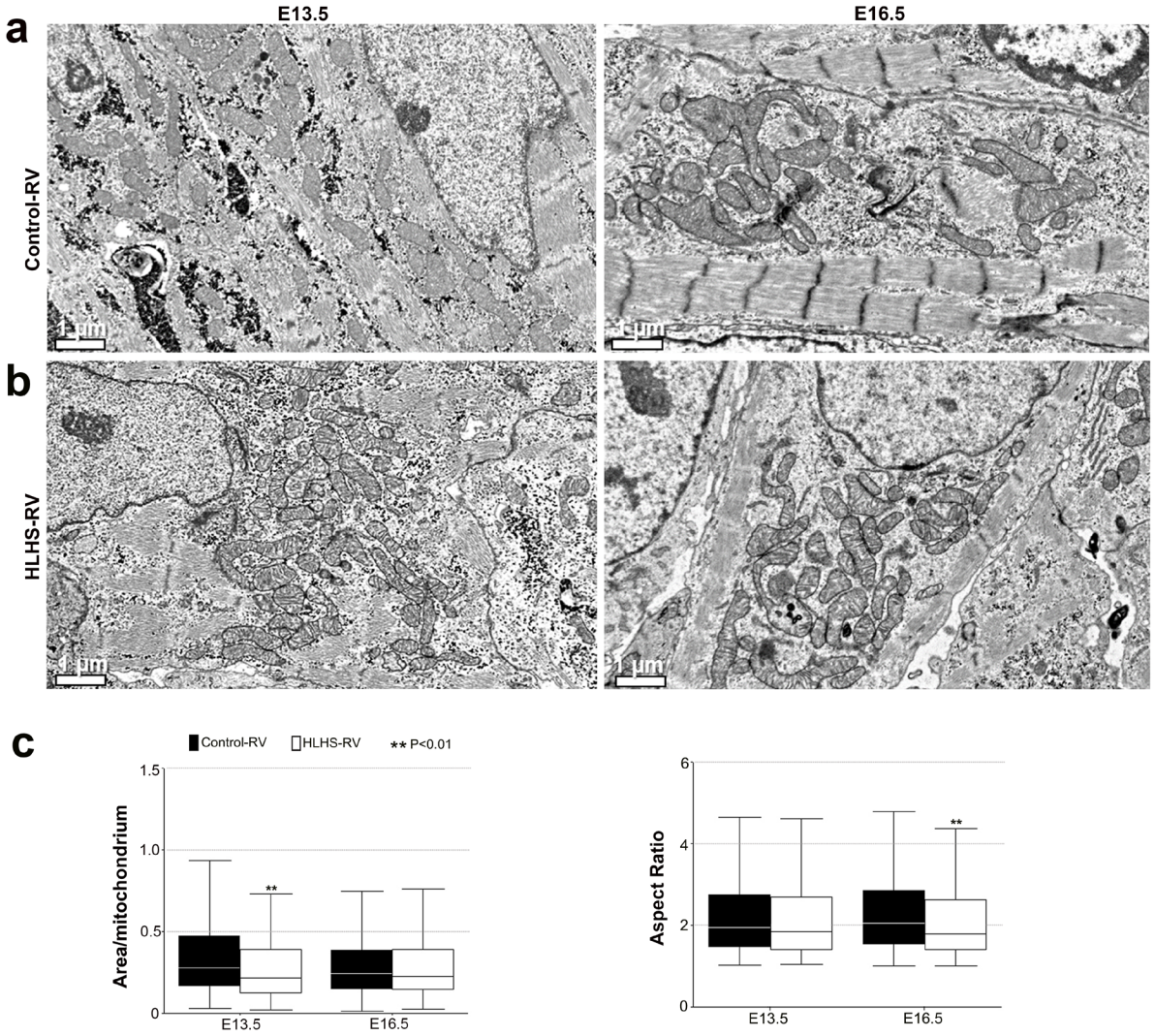

Supplementary Figure 12. Electron microscopy of *Ohia* HLHS-RV

(a,b). Electron microscopy of E13.5 and E16.5 HLHS-RV (b) vs. control-RV (a). HLHS-RV at E13.5 exhibited shorter myofibrils with less distinct z-bands, and have mitochondria with low density matrix and sparse cristae. The HLHS-RV at E16.5 appeared more similar to the control-RV. Inset: enlarged view of boxed regions. Scale bar: 1um.

(c,d). Quantification showed mitochondria in HLHS-RV were smaller at E13.5, but becoming more rounded at E16.5. Number of mitochondria analyzed: E13.5-control,n=507 and HLHS,n=271 and E16.5- control,n=960 and HLHS,n=569. Wilcoxon rank-sum test, for mitochondrial area: E13.5, P=0.000108; E16.5, P=0.462; for aspect ratio: E13.5, P=0.426; E16.5, P=0.000004.

Nature Genetics: doi:10.1038/ng.3870

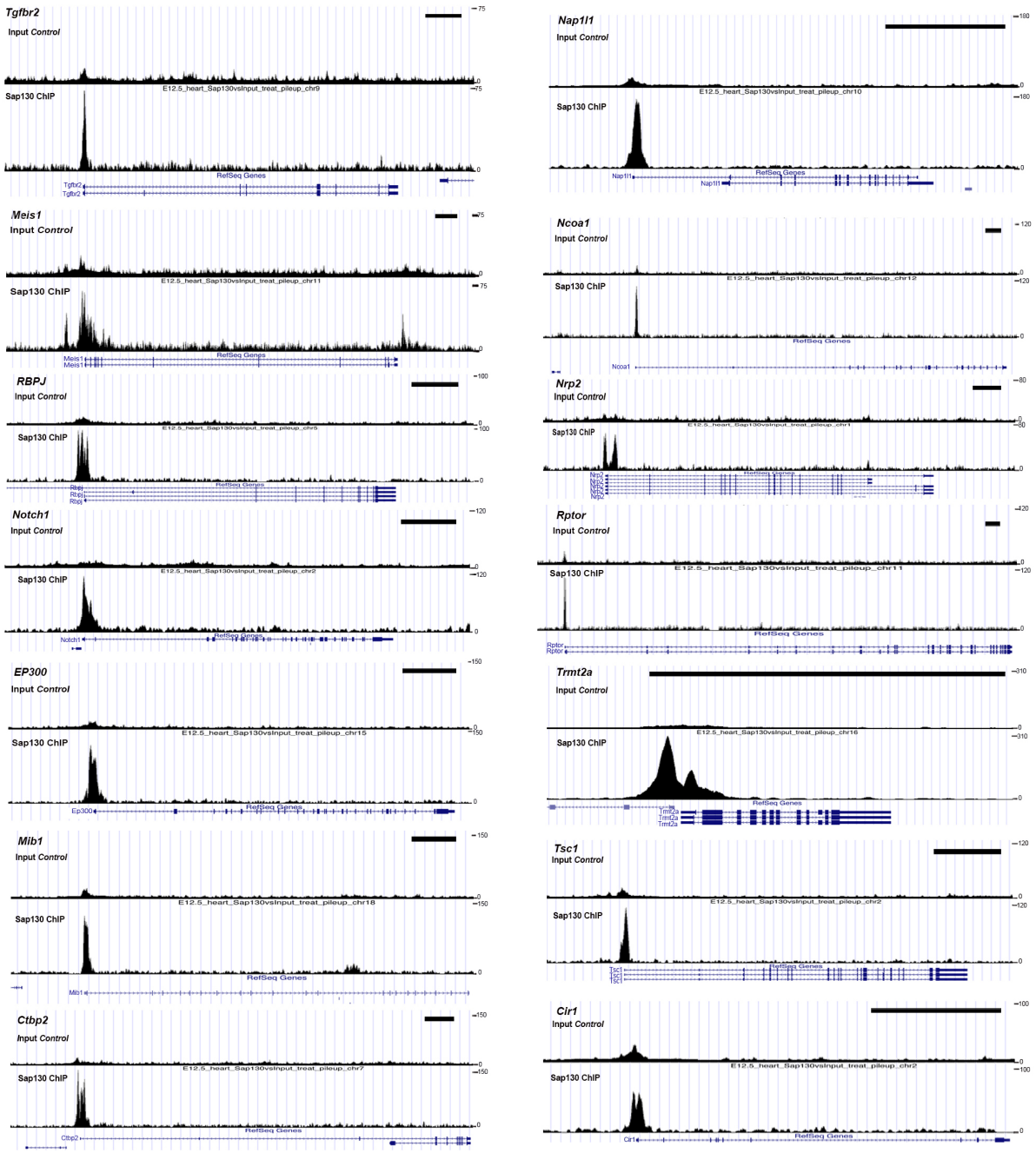

Supplementary Figure 13. Sap130 occupancy profile over selected target genes

Sap130 ChIP-seq peaks observed in the promoter region of various genes. Scale bar=10kb.

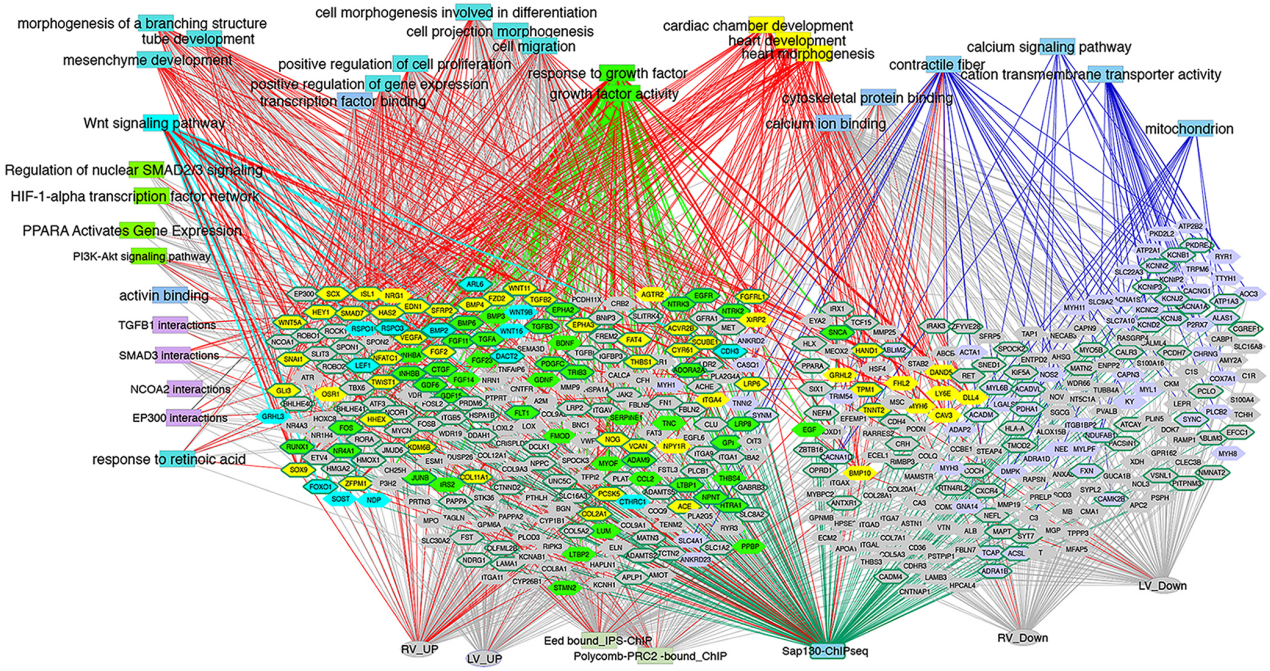

Supplementary Figure 14. Interactome network comprising differentially expressed genes recovered by RNAseq and *Sap130* ChIP-seq analysis of *Ohia* mutant heart tissue.

ToppCluster network analysis of genes (hexagons) that are differentially expressed in the hearts of HLHS mice based on RNAseq analysis, or identified as *Sap130* targets by ChIP-seq analysis of E12.5 mouse heart. Genes highlighted in yellow are associated with cardiac development terms. Associations of these genes are indicated by red edges into other functional categories that include GO biological process and cellular component, pathways, or mouse knockout allele phenotype associations as determined by ToppGene. Genes that are *Sap130* targets are shown surrounded with green edges. Genes associated with other enriched functional categories such as growth factor signaling, Wnt signaling, or mitochondrial function are colored individually with matching edges, except when they are linked to cardiac morphogenesis, in which case the edges are in red.

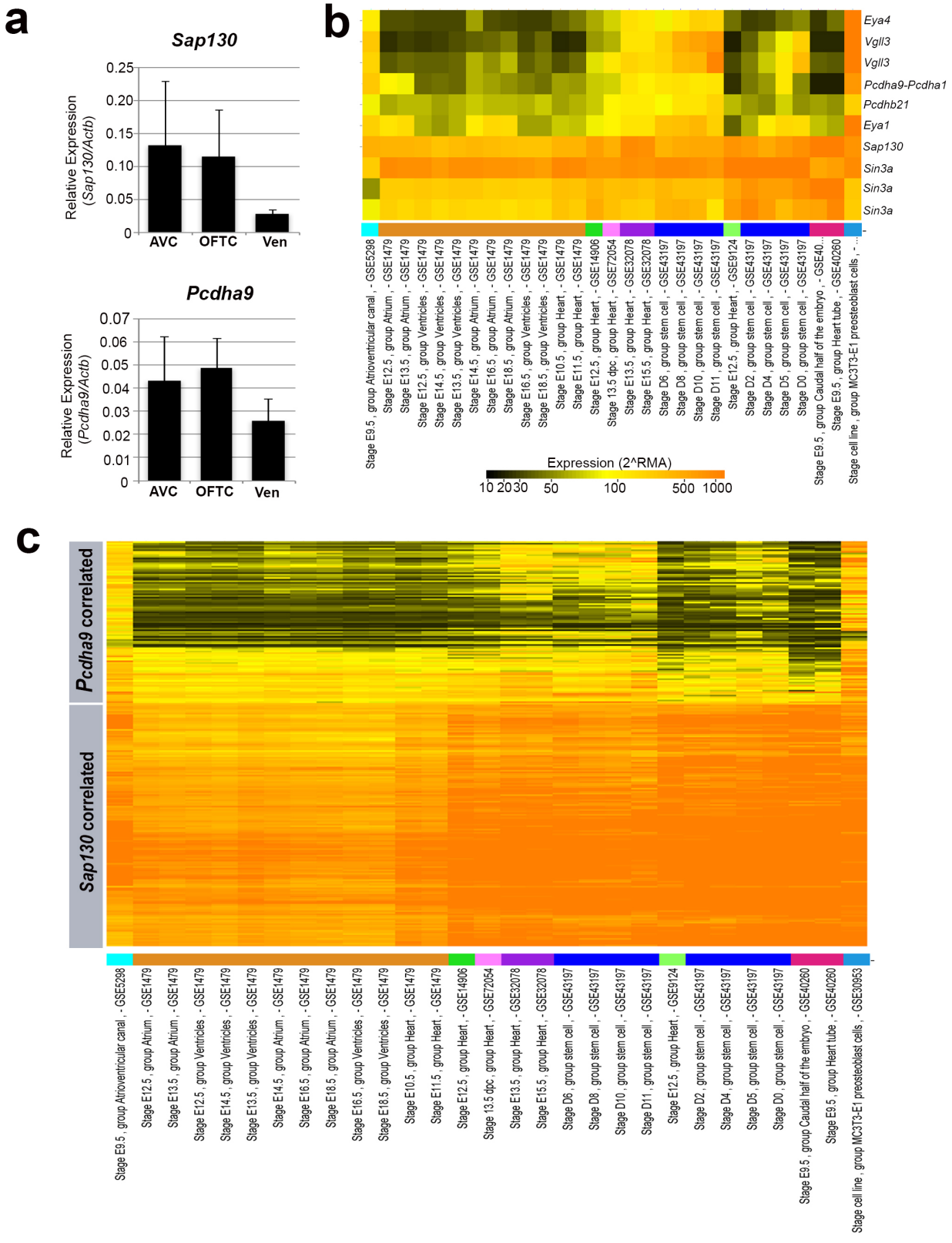

Supplementary Figure 15. *Sap130* and *Pcdha9* expression patterns and coregulated genes in

embryonic cardiac cushion and developing heart-related tissue samples.

(a). Real time PCR analysis of *Pcdha9* and *Sap130* gene expression in microdissected mouse E10.5 atrioventricular (AVC) (n=4) and outflow tract (OFTC) (n=4) cushion tissues and the common ventricle (Ven) (n=4).

(b,c). Identification of *Pcdha9* and *Sap130* co-regulated gene modules in developing heart tissues was identified using microarray data encompassing heart tissue from a wide range of developmental stages and encompassing different regions, compartments and cell differentiation models of the heart making up a Cardiomic Gene Expression Atlas (see Methods) [26-33].

Pcdha related and *Sap130* probes were identified from the microarray dataset (b), with the strongest *Pcdha9* expression seen in E9.5 atrioventricular canal. In panel (c), the *Pcdha9/Sap130* coregulated genes are identified, with the upper heatmap showing *Pcdha9*-correlated probe sets, and lower heat map showing *Sap130*-correlated probe sets.

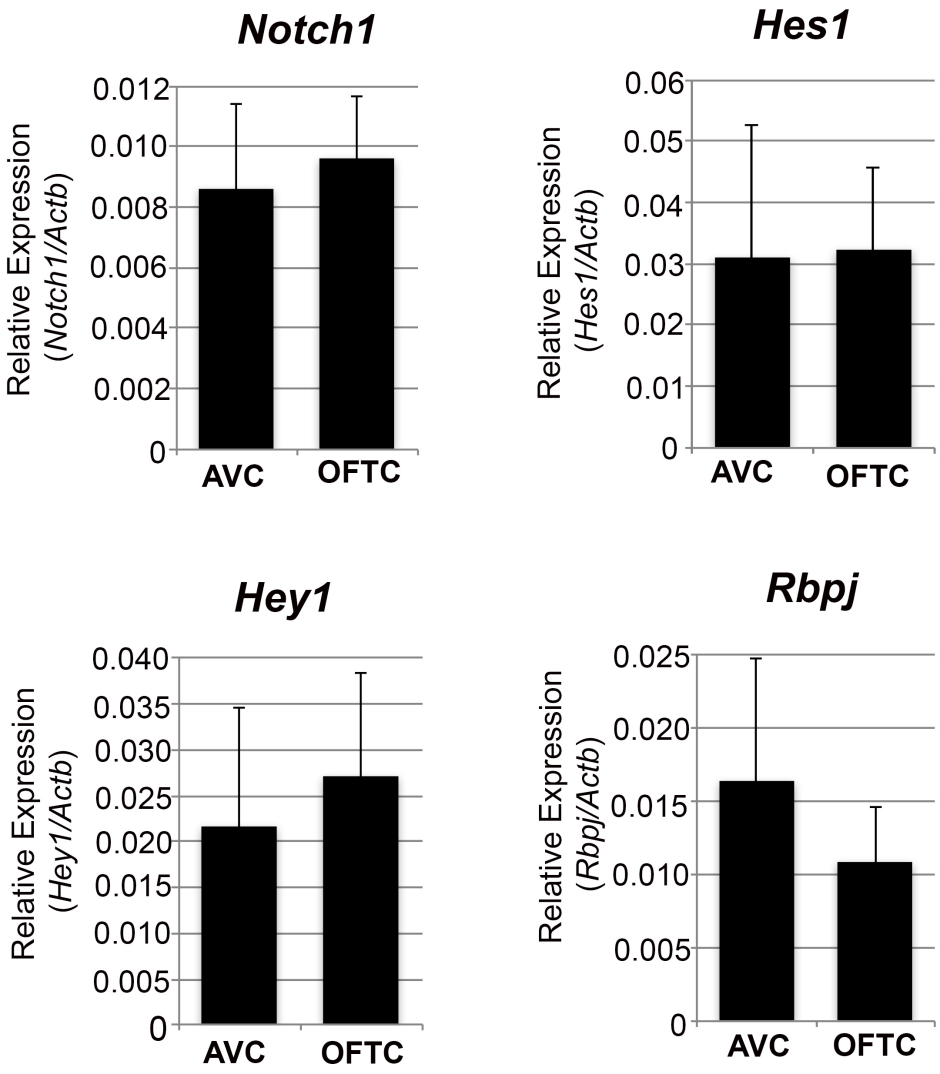

Supplementary Figure 16. Expression of *Notch* and downstream genes regulating cardiac valve development in E10.5 AV and OFT cushions.

Quantitative PCR analysis of the atrioventricular cushion (AVC) and outflow tract cushions (OFTC) in wildtype C56BL/6J embryos at E10.5 showed expression of *Notch* and downstream genes in both AVC (n=4) and OFTC (n=4) cushion tissue. Shown are mean±s.d.

Nature Genetics: doi:10.1038/ng.3870

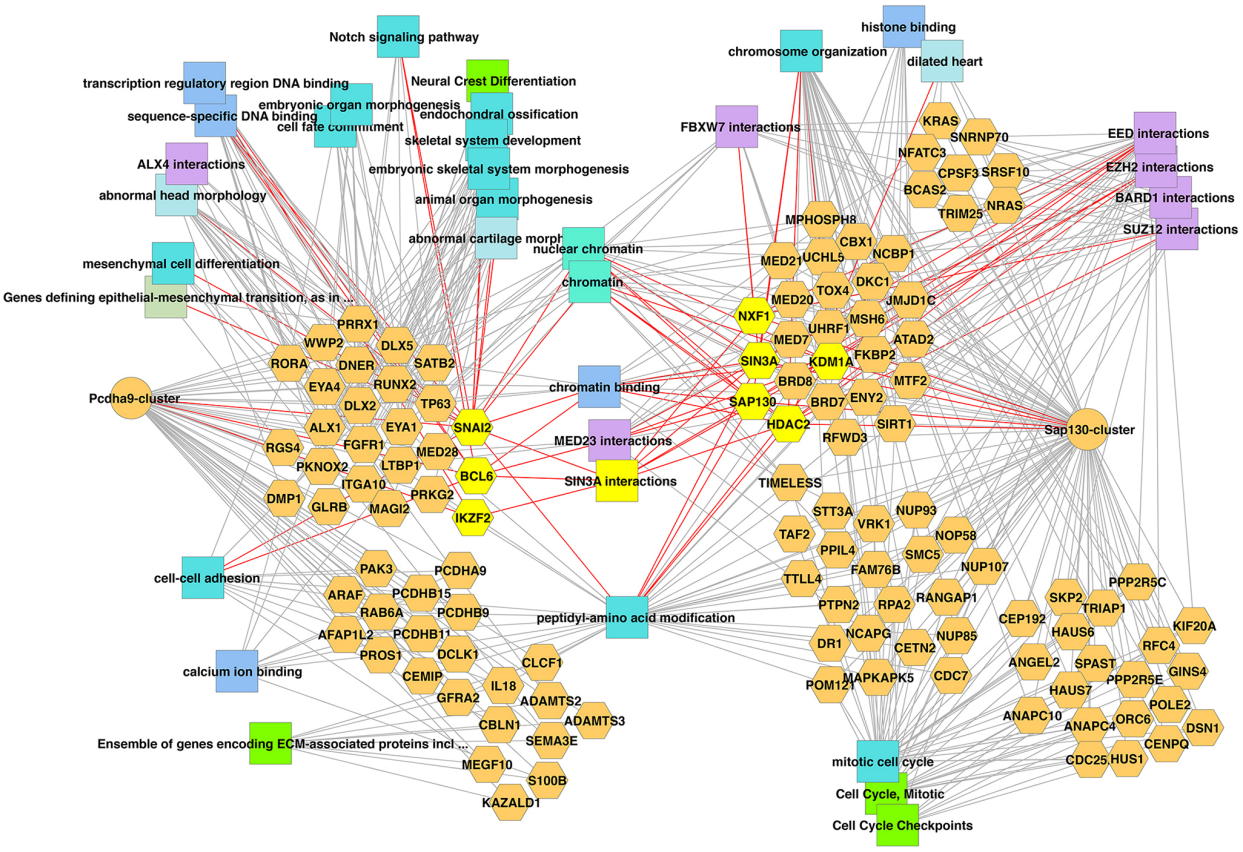

Supplementary Figure 17. Multidimensional feature enrichment and functional interaction network analysis of Pcdha9 and Sap130-correlated genesets identified in developing heart. Feature enrichment and interaction networks of *Pcdha9* and *Sap130* coregulated gene modules in the embryonic mouse heart development were constructed using ToppCluster analysis[25]. (see Supplementary Fig S15). The *Pcdha9* coregulated gene module is highly enriched for sequence-specific transcription factors and chromatin, Notch pathway, embryonic structure morphogenesis, mesenchymal epithelial transition, and calcium binding and cell-cell adhesion. In contrast, the *Sap130* coregulated gene module network on the right combines chromatin organization, cell cycle, and many interactions associated with *Med23*, *Sin3a*, and *Ezh2* among others. The interacting terms shown in the middle are those shared by genes specific to either the *Sap130* or *Pcdha9* networks. Genes found in both networks that are associated with Sin3a Polycomb repression are highlighted with yellow fill and the red edges delineate the concepts, pathways, and interactions that they are associated with.

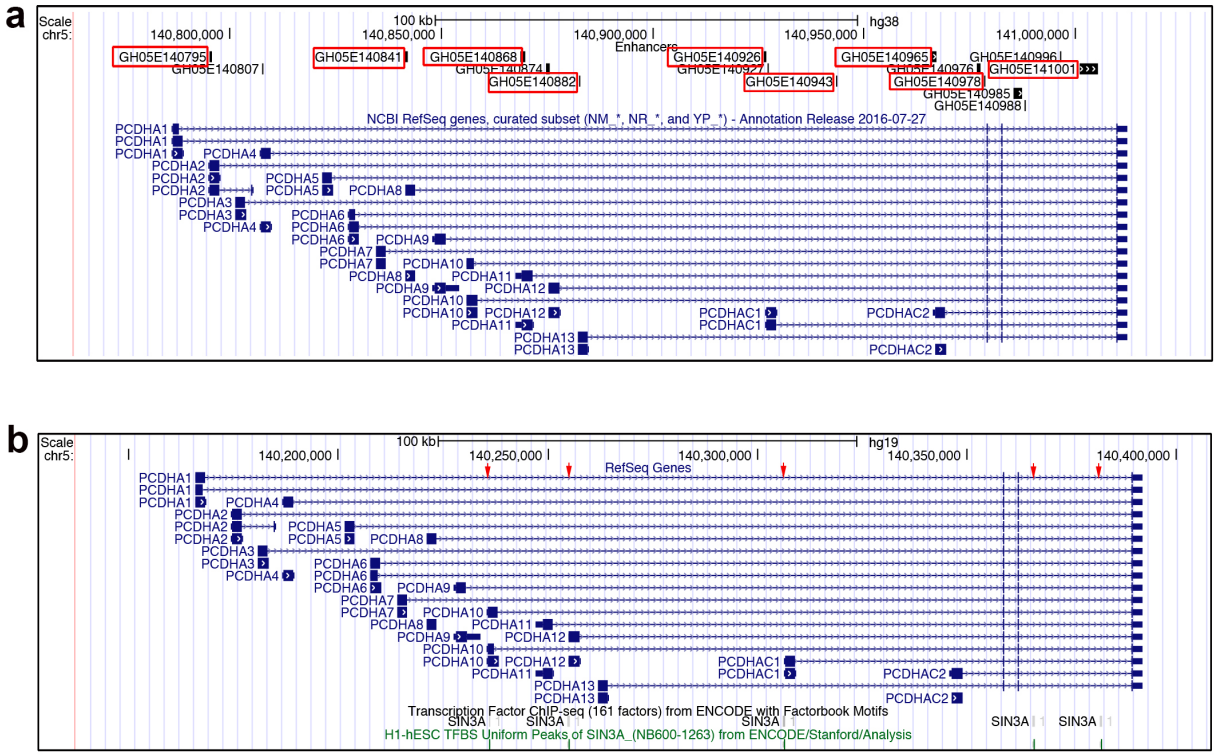

Supplementary Figure 18. SIN3A binding sites in the *PCDHA* gene cluster.

a. Genomic regulatory element near *PCDHA* gene cluster from GeneHancer database on hg38 genome assembly (See URL blow). Elements shown in red open square has SIN3A binding site[1-4].

http://genome.ucsc.edu/cgi-bin/hgTracks?db=hg38&lastVirtModeType=default&lastVirtModeExtraState=&virtModeType=default&virtMode=0&nonVirtPosition=&position=chr5%3A140776136%2D141022347&hgsid=584910445_S0AwJT48ltXNVs0hxRhBkWdtADBf

b. ENCODE SIN3A ChIP-seq data from H1 hES cell line shown with Factorbook Motifs on hg19 genome assembly. Five SIN3A binding sites are found in the *PCDHA* gene cluster. Red arrows denote approximate position of SIN3A binding sites[1,5].

1 Consortium, E. P. An integrated encyclopedia of DNA elements in the human genome. *Nature* **489**, 57-74, doi:10.1038/nature11247 (2012).
2 Zerbino, D. R., Wilder, S. P., Johnson, N., Juettemann, T. & Flicek, P. R. The ensembl regulatory build. *Genome Biol* **16**, 56, doi:10.1186/s13059-015-0621-5 (2015).
3 Andersson, R. *et al.* An atlas of active enhancers across human cell types and tissues. *Nature* **507**, 455-461, doi:10.1038/nature12787 (2014).

4 Visel, A., Minovitsky, S., Dubchak, I. & Pennacchio, L. A. VISTA Enhancer Browser--a database of tissue-specific human enhancers. *Nucleic Acids Res* **35**, D88-92, doi:10.1093/nar/gkl822 (2007).
5 Consortium, E. P. A user's guide to the encyclopedia of DNA elements (ENCODE). *PLoS Biol* **9**, e1001046, doi:10.1371/journal.pbio.1001046 (2011).

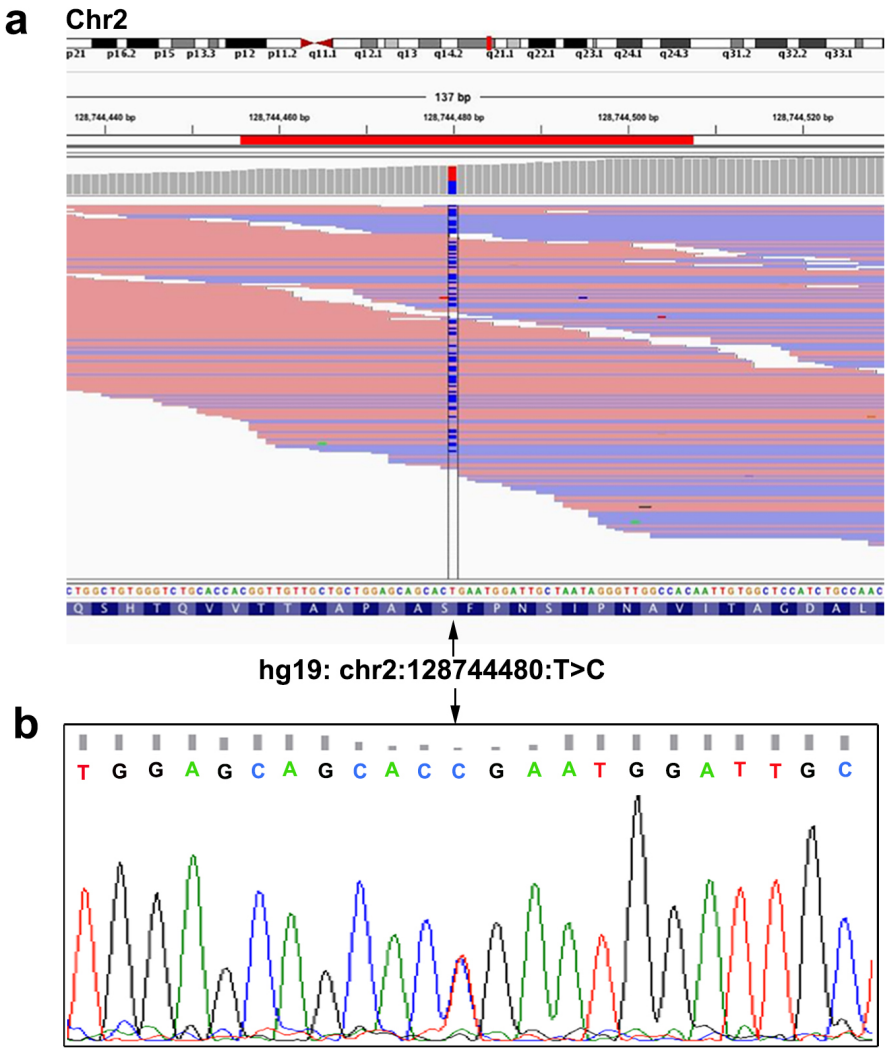

Supplementary Figure 19. *Sap130* coding variant identified in patient HLHS-22 by Illumina and Sanger sequencing.

Sap130 mutation (Chr 2: 128744480 T>C, p. S639G) of patient HLHS-22 recovered from whole exome sequencing (a, arrow) analysis was validated by Sanger sequencing (b, arrow).

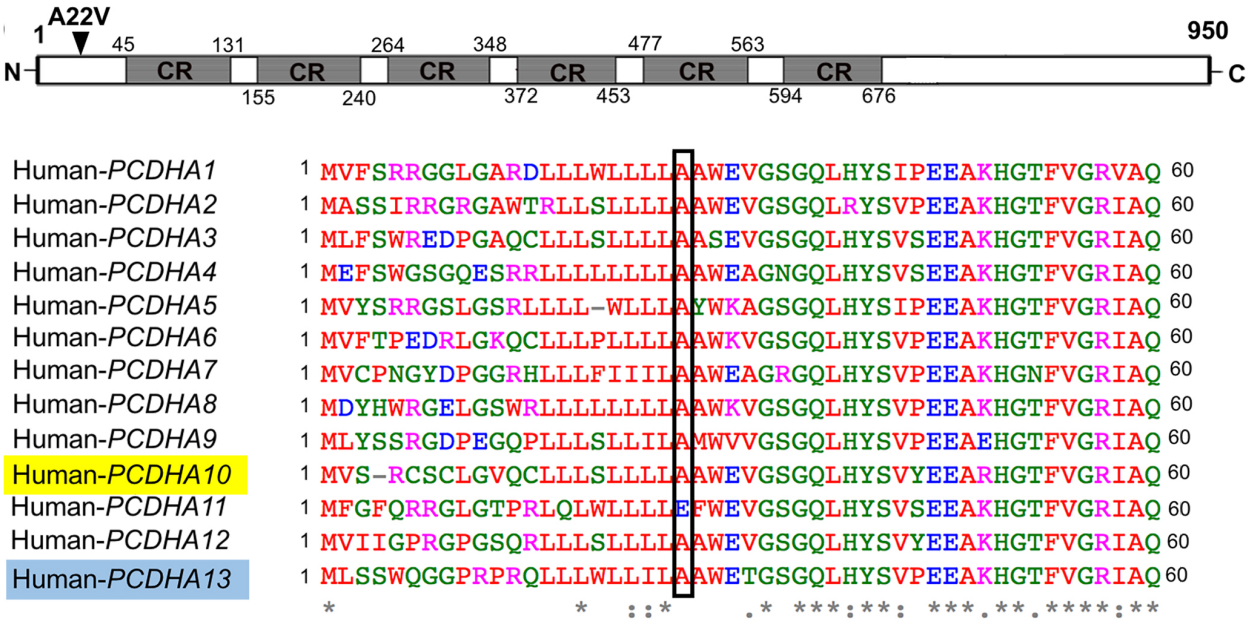

Supplementary Figure 20. *PCDHA13* mutation in patient HLHS-22

PCDHA13 missense mutation found in patient HLHS-22 (arrowhead) who also had a *SAP130* mutation. The mutation (highlighted in blue) is within a region that is highly homologous across the *PCDHA* gene family (black box), including human *PCDHA10* (highlighted in yellow), the ortholog of mouse *Pcdha9,* the gene mutated in the *Ohia* HLHS mouse mutant.

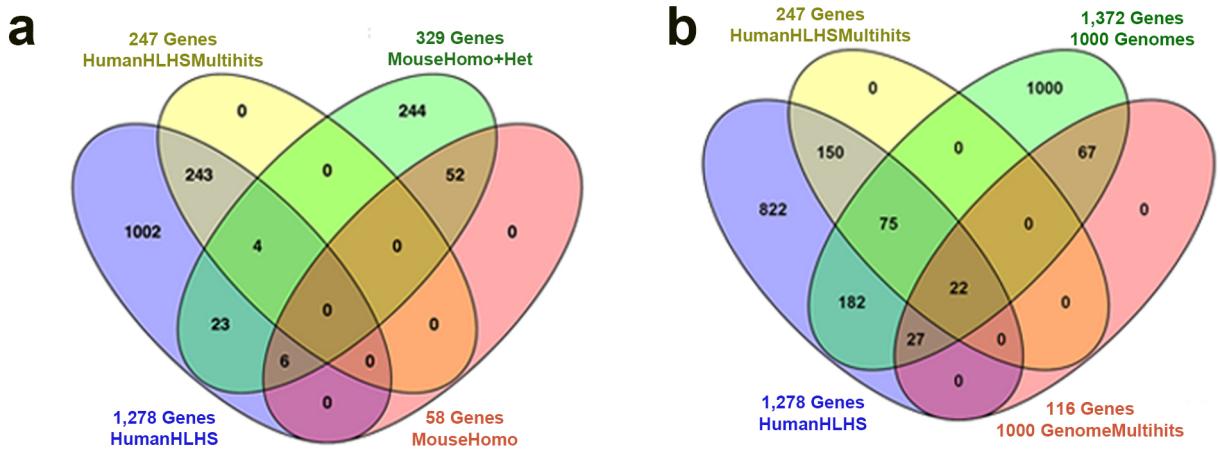

Supplementary Figure 21. Sharing of multihit genes in HLHS patients and CEU controls, and overlap with mutations in HLHS mutant mice

(a). Venn diagram shows overlap in genes with unique loss-of-function (LOF) variants in the HLHS patients (blue) vs. the subset that are multihit (genes with unique LOF found in two or more subjects) (Yellow) and their overlap with mouse homozygous (red) or homozygous+heterozygous mutations (green) recovered in the 8 independent HLHS mutant lines.

(b). Venn diagram shows overlap of genes with LOF variants (blue) and multihit genes (yellow) found in HLHS patients vs. unique LOF (green) and multihit (red) genes found in 1000 Genomes control subjects.

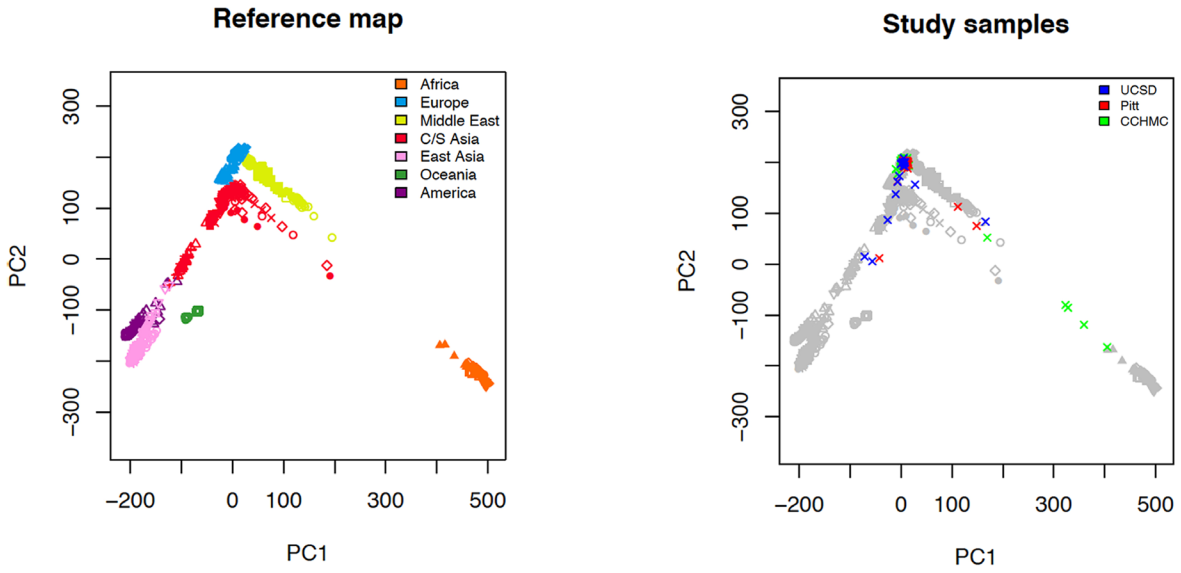

Supplementary Figure 22. Ethnicity in HLHS patents relative to 1000 Genome subjects

LASER (Locating Ancestry from SEquence Reads) analysis of patient ancestry in the different HLHS population relative to samples from the Human Genome Diversity Project (http://csg.sph.umich.edu/chaolong/LASER/). Note the 68 HLHS patients were mostly white, showing overlap largely with CEU subjects from Europe.

SUPPLEMENTARY TABLES

Supplementary Table 1. HLHS Transmission in 8 Independent Mouse Lines

Line ID	No. G2 Females[1]	No. Litters[2]	No. Fetuses[3]	No. HLHS Mutants	HLHS Incidence[4]
464	5	20	147	1	0.68%
	464-003	3	18	1	5.56%
635	5	25	163	2	1.23%
	635-004	6	45	2	4.44%
1430	6	22	128	1	0.78%
	1430-014	2	17	1	5.88%
1432	4	23	142	1	0.70%
	1432-005	4	27	1	3.70%
1709	5	16	103	1	0.97%
	1709-003	4	21	1	4.76%
1963	5	12	75	1	1.33%
	1963-002	1	8	1	-
3077	5	11	68	1	1.47%
	3077-006	1	6	1	-
3183	5	8	35	1	2.86%
	3183-006	1	2	1	-
TOTAL	40	137	861	9	1.05%

[1]No. G2 females: Top row for each line represents the total number of G2 females in a G1 pedigree (identified by Line ID) that were ultrasound screened. The second row shows the specific G2 female from which the HLHS mutant was recovered.
[2]No. Litters: Total number of litters ultrasound screened, either encompassing all G2 females from the line (top row), or the specific G2 female from which the HLHS fetus was recovered (bottom row).
[3]No. Fetuses: Top row shows total number of fetuses recovered from all G2 females mated to the G1 male in each pedigree. Bottom row shows number of fetuses recovered from the G2 female that yielded the HLHS mutant.
[4]Incidence is derived from number of HLHS mutants observed divided by total number of fetuses screened. This was only calculated for lines in which multiple litters from the same G2 female yielding the HLHS mutant were ultrasound screened.

Nature Genetics: doi:10.1038/ng.3870

Supplementary Table 2. Lethality of *Sap130*$^{-/-}$ and *Sap130*$^{m/m}$ Embryos[a]

Stage	*Sap130*$^{+/+}$	*Sap130*$^{+/-}$	*Sap130*$^{-/-}$	Total No. Embryos
E7.5	3	7	0	10
E8.5	7	10	0	17
E9.5	2	13	0	15
E10.5	6	6	0	12
E11.5	1	6	0	7
E13.5	8	8	0	16
P0	13	19	0	32
Total (%)	**40 (37%)**	**69 (63%)**	**0**	**109**

Stage	*Sap130*$^{+/+}$	*Sap130*$^{+/m}$	*Sap130*$^{m/m}$	Total No. Embryos
E12.5	2	2	6	10
E13.5	9	3	6	18
E14.5	6	15	9	30
E15.5	8	8	7	23
E17.5	2	1	1	4
Total (%)	**27 (31%)**	**29 (34%)**	**29 (35%)**	**85**

Stage	*Sap130*$^{+/+}$	*Sap130*$^{+/m}$	*Sap130*$^{+/-}$	*Sap130*$^{m/-}$	Total No. Embryos
E9.5	7	5	8	0	20

[a]*Sap130*$^{-/-}$: homozygous *Sap130* knockout; *Sap130*$^{m/m}$: homozygous for *Ohia Sap130* allele ; *Sap130*$^{m/-}$: heterozygous for *Ohia* and knockout *Sap130* alleles.

Supplementary Table 3 *SAP130* and *PCDHA* Mutations in HLHS Patients

ID	Gene	Position	Base	AA	ExAC MAF	RS ID
SAP130						
HLHS-22	*SAP130*	Chr2:128744480	T>C	S639G	0.006619	rs72841716
PCDHA						
HLHS-63	*PCDHA1*	Chr5:140167220	A>C	N449H	0.004294	rs3733712
HLHS-36	*PCDHA2*	Chr5:140176641	G>A	V698M	0.001594	rs151049201
HLHS-18	*PCDHA3*	Chr5:140182240	G>T	E486D	5.00E-05	.
HLHS-23	*PCDHA3*	Chr5:140183237	A>G	T819A	0.008711	rs17844265
HLHS-51	*PCDHA3*	Chr5:140180926	C>G	I48M	8.00E-06	.
HLHS-24	*PCDHA6*	Chr5:140210033	C>T	A786V	0.006482	rs150956127
HLHS-39	*PCDHA6*	Chr5:140209679	C>T	S668L	NA	.
HLHS-5	*PCDHA7*	Chr5:140216051	G>T	D695Y	NA	.
HLHS-59	*PCDHA7*	Chr5:140215350	C>T	T461M	NA	.
HLHS-21	*PCDHA9*	Chr5:140230187	G>T	A703S	0.000158	rs146973370
HLHS-32	*PCDHA9*	Chr5:140230382	G>T	D768Y	0.00015	rs146333783
HLHS-56	*PCDHA10*	Chr5:140237650	C>T	Q673*	0.001634	rs200661444
HLHS-58	*PCDHA10*	Chr5:140238055	T>C	F808L	0.006566	rs73793505
HLHS-37	*PCDHA11*	Chr5:140248791	G>C	V35L	0.00308	rs192388233
HLHS-63	*PCDHA12*	Chr5:140256988	G>A	R644H	0.0001572	rs199806507
HLHS-22	*PCDHA13*	Chr5:140261918	C>T	A22V	NA	.
HLHS-63	*PCDHA13*	Chr5:140263489	G>A	G546S	0.003458	rs146827381

Supplementary Table 4. Sharing Genes with Loss-of-Function Mutations in HLHS Patients and Mice

Comparison[a]		No. Shared Genes with Unique LOF			P value[b]	Inference
Group 1	Groups 2	Observed	Expected	Observed/ Expected		
hHLHS	mHLHS	33	22	1.50	0.013	More sharing than by chance
CEU	mHLHS	28	22	1.27	0.21	Chance sharing
hHLHS		247	69	3.57	9.1×10^{-24}	More sharing than by chance
CEU		116	265	0.44	4.5×10^{-16}	Less sharing in CEU than expected
hHLHS	CEU	306	453	0.67	4.2×10^{-7}	Less sharing in CEU than HLHS

[a]Comparison includes 68 HLHS (hHLHS) patients, and 95 1000 genomes ethic matched CEU subjects, and 8 independently derived HLHS mutant mice (mHLHS). The HLHS patients had 1,278 genes with 1,736 unique LOF, while the 1000 genomes CEU subjects had 1,372 genes with 1,550 unique LOF. Unique LOF are seen in only a single subject in the HLHS or CEU cohort. The 8 HLHS mutant mice in total had 329 mutations in 329 genes.
[b]Comparisons between groups was performed with χ^2 goodness of fit tests.

Supplementary Table 5. Loss of Function Variants in *Notch* Related Genes

Patient ID	Gene	Position	Base	CADD	ExAC MAF	RS ID
HLHS-1	*MIB1*	Chr18:19437181	C>G	39	NA	NA
HLHS-28	*PTCRA*	Chr6:42893157	C>T	35	0.000364	rs542853935
HLHS-29	*CTBP2*	Chr10:126678207	GA>G	35	0.000711	rs748974251
HLHS-35	*CTBP2*	Chr10:126678204	G>GA	35	0.000705	rs35551618
HLHS-35	*RFNG*	Chr17:80009200	C>CG	33	2.20E-05	rs749555015
HLHS-37	*TNRC6B*	Chr22:40552117	A>G	24.9	3.20E-05	rs146996627
HLHS-45	*MIB1*	Chr18:19359544	GA>G	25.8	8.00E-06	rs770127974
HLHS-54	*RBPJ*	Chr4:26417145	GA>G	33	5.80E-05	rs761285857
HLHS-56	*MIB1*	Chr18:19437141	C>T	45	6.60E-05	rs201146927
HLHS-59	*CIR1*	Chr2:175213870	CT>C	33	NA	NA
HLHS-60	*CIR1*	Chr2:175213712	AT>A,ATT	21.9	0.000103	rs752412345
HLHS-63	*SPEN*	Chr1:16255141	GGA>G	33	0.000174	rs764595221

Supplementary Table 6. Loss of Function Variants in *Tgfβ* Related Genes

ID	Gene	Position	Base	CADD	ExAC MAF	RS ID
HLHS-16	*THBS3*	Chr1:155165670	CAA>C	35	NA	rs567801958
HLHS-25	*E2F5*	Chr8:86127232	ACT>A	26.1	0.000335	rs540894179
HLHS-37	*SMAD9*	Chr13:37441408	A>T	20.8	9.20E-05	rs770716081
HLHS-53	*PPP2R1B*	Chr11:111631737	AAC>A	33	7.00E-04	rs528568533
HLHS-54	*APOA1*	Chr11:116706794	GGC>G	23.4	0.000118	rs781350389
HLHS-54	*GDF6*	Chr8:97157409	CCG>C	24.6	0.000888	rs763824384
HLHS-56	*RBL1*	Chr20:35684584	GTA>G	35	NA	NA
HLHS-58	*SMAD6*	Chr15:67073393	G>A	41	NA	NA

Supplementary Table 7. Oligonucleotide Sequences

Name	Oligonucleotide sequences
Ohia Sap130 genotype primers	F- tttttaccctcttttcaggatct; R- aagtcaaattcagagttgctttg
Ohia Pcdha9 genotype primers	F- tgctcacgctgctgctatac; R- cgcattgttaaaaatacttgtgc
Ohia Pepd genotype primers	F- tagcccaggcagagcttaaa; R- gcggtgtctgtcagtcaaga
Ohia Nadsyn1 genotype primers	F- atgggtaccctgaagctcct; R- tctcttcagcggctatggat
*Ohia Esco1*genotype primers	F- tgtgatgcaaagtgacacaaa; R- gctccagagggtgacttaagatt
Mouse CRISPR/Cas9 Forward Guide Primer 5'->3'	*Sap130*: gaaattaatacgactcactataggCATGTCCAACACTTACCAACg ttttagagctagaaatagc *Pcdha9*: gaaattaatacgactcactataggTCCGCCCAAAACCGACCTCAgt tttagagctagaaatagc
Mouse Single-stranded oligonucleotides donors(ssODN)	*Sap130*: tcatcccatgctactgctgtgaccacttcaaatatcccagttggCaagtgtt ggacatgtcgcacaaaagcctttgaggaatttgcaggc *Pcdha9*: gtggggacctggtcatactcacagcagagacagcagcgagtatgctcag gagagggtcTgccTaaGaccgacTtGatggcttttagccccagtcttac accttgcccagtggccgaagt
Mouse CRISPR/Cas9 *Sap130* genotype primers	F-cccaagaactttcccaaggt; R-tgcatatatactgaacacagacacaga
Mouse CRISPR/Cas9 *Pcdha9* genotype primers	F-tgctcacgctgctgctatac; R-cgcattgttaaaaatacttgtgc
Zebrafish *sap130a* (5ng) translation blocking	5'ccacaacatagtgtgaatactgcat3'
Zebrafish *sap130a* CRISPR/Cas9 Forward Guide Primer 5'->3'	5'-gagggaggcagagcagctcg-3'
Zebrafish CRISPR/Cas9 *sap130a* genotype primers	F-aattaggattgaatagcgcagg R- cctcctacctgaatgtgttcct
Mouse heart RT-PCR primers	*Sap130* F- agcagccccaatcaacact;R-catctgccaacaccactga; *Pcdha9*: F-ctctggtgtcaatggacaggt;R-caccaacttgaaggggacat; *β-actin*: F-ctaaggccaaccgtgaaaag;R-accagaggcatacagggac

Splicing analysis of mouse *Sap130* mutation	Sap130-Exon 8-F:cggcccactttatctatcca; Sap130-Exon12-R:agtggacacagagctggtga
HLHS-22 *Sap130* mutation genotype	F- cagtctcagctgggtaaggc R- tgtcggatgaacattgtgct
Mouse AV cushion RT-PCR primers of *Notch1*	F- ggatgctgactgcatggat R- aatcatgaggggtgtgaagc
Mouse AV cushion RT-PCR primers of *Hey1*	F- ctgtggcctcgctctcag R- ggtgtcgaagggctcagtag
Mouse AV cushion RT-PCR primers of *Hes1*	F- acaccggacaaaccaaagac R- cgcctcttctccatgatagg
Mouse AV cushion RT-PCR primers of *Rbpj*	F- ggcagtgtccttgggtacag R- ggttaagatggtggcaggaa